



Cite this: *Nanoscale*, 2017, 9, 16638

Received 20th July 2017,
 Accepted 2nd October 2017

DOI: 10.1039/c7nr05325h

rsc.li/nanoscale

Nanostructured topological state in bismuth nanotube arrays: inverting bonding–antibonding levels of molecular orbitals†

Kyung-Hwan Jin,^a Seung-Hoon Jhi^b and Feng Liu*^{a,c}

We demonstrate a new class of nanostructured topological materials that exhibit a topological quantum phase arising from nanoscale structural motifs. Based on first-principles calculations, we show that an array of bismuth nanotubes (Bi-NTs), a superlattice of Bi-NTs with periodicity in the order of tube diameter, behaves as a nanostructured two-dimensional (2D) quantum spin Hall (QSH) insulator, as confirmed from the calculated band topology and 1D helical edge states. The underpinning mechanism of the QSH phase in the Bi-NT array is revealed to be inversion of bonding–antibonding levels of molecular orbitals of constituent nanostructural elements in place of atomic-orbital band inversion in conventional QSH insulators. The quantized edge conductance of the QSH phase in a Bi-NT array can be more easily isolated from bulk contributions and their properties can be highly tuned by tube size, representing distinctive advantages of nanostructured topological phases. Our finding opens a new avenue for topological materials by extending topological phases into nanomaterials with molecular-orbital-band inversion.

In the past few decades, we have witnessed several emerging frontier areas of materials research, *e.g.*, from nanostructures/nanomaterials¹ to graphene/2D materials² and to 2D/3D topological materials.^{3–8} Generally, nanostructures exhibit strong size-dependent properties arising from the quantum confinement effect and a large varying surface/volume ratio. On the

other hand, the topological order of a solid material is inherently linked to its band topology of Bloch states; hence a topological material is implicitly referred to as a crystalline material with long-range translational order. Consequently, so far there are only very few studies of topological phases in nanostructures and nanomaterials.^{9–11} Two recent studies reported interesting topological states formed in a 1D nanowire/nanoribbon due to the Rashba type of spin–orbit coupling (SOC) induced by an external field⁹ or structural helicity.¹⁰ Another study reported topological states in a nanopatterned semiconductor of GaAs.¹¹

There are usually three key ingredients to realize a topological quantum phase in a 2D or 3D crystalline solid: lattice symmetry, SOC and atomic orbitals associated with band-edge states,^{12,13} which conspire to induce a band-edge parity inversion around the Fermi level. (For a Chern insulator of anomalous quantum Hall effect (QAHE), the exchange interaction is another ingredient to be considered.¹⁴) Especially, in the presence of inversion symmetry, it is commonly required that the atomic or molecular orbitals associated with the valence band maximum (VBM) and conduction band minimum (CBM) must be of opposite parity so that they will exchange parity upon band inversion. More generally, in systems without inversion symmetry, parity is no longer well defined, and band inversion will manifest in exchanges of different orbital characters (*s*-*p*,¹⁵ *p*-*p*¹⁶ or bonding and antibonding band-edge states¹²). We note that these same ingredients can also be applied to induce topological phases in nanopatterned structures. For example, in ref. 11, the topological phase arises from a patterned artificial honeycomb lattice with atomic *p*^{3/2} orbital parity inversion induced by the confinement effect. In this sense, it is mechanistically related to the classical Kane–Mele model in terms of a hexagonal lattice and SOC⁴ and the Bernevig–Hughes–Zhang quantum-well⁵ model in terms of confinement induced atomic-orbital band inversion.

On the other hand, there exists a wide class of nanostructured materials made of the assembly of individual nanostructures, which can have long-range translational order with a super periodicity in the range of the size of the given nano-

^aDepartment of Materials Science and Engineering, University of Utah, Salt Lake City, UT 84112, USA. E-mail: fliu@eng.utah.edu

^bDepartment of Physics, Pohang University of Science and Technology, Pohang 790-784, Korea

^cCollaborative Innovation Center of Quantum Matter, Beijing 100084, China

† Electronic supplementary information (ESI) available: The notation of Bi-NTs, the interaction strength of intertube coupling, other possible intertube bonding geometries, the robustness of QSH against the structural disorder and calculated phonon spectra, the calculated Z_2 topological invariant of Bi-NT arrays, the band structure using a hybrid functional, the effective model for the Bi-NT array, the molecular bonding and antibonding orbitals of Bi-NTs, the charge redistribution at the junction point, the localization length of edge states, the QSH phase of various Bi-NT arrays, the calculated band structure of Bi-NT arrays on the BN sheet and nontrivial edge state of a curved Bi-NT array. See DOI: 10.1039/c7nr05325h

structures in a perfectly ordered phase, but they may not have a simple lattice symmetry (*e.g.*, nanotube arrays) and their electronic bands are no longer derived from atomic basis but molecular orbitals of constituent nanostructures with a linear combination of atomic orbitals, whose parity is *a priori* unknown. Well-known examples include C_{60} ¹⁷ and cluster-assembled solids,^{18–20} a bundle^{21,22} and array of nanotubes,²³ colloidal solids,²⁴ *etc.* Therefore, a very interesting question is whether such nanostructured material can still exhibit nontrivial topological order when mechanisms of lattice symmetry and band inversion are not obviously in play. The answer to this question will significantly not only advance the basic knowledge of topological physics by discovering new mechanisms underlying the topological order (*e.g.*, inversion of molecular orbitals *vs.* atomic orbitals), but also expand the scope of topological materials and their potential applications into a new class of nanomaterials.

As the first attempt, we choose the 2D array of bismuth nanotubes (Bi-NTs) as an illustrative example of study. Bismuth, having among the largest atomic SOCs, is the most common element involved in TIs and it induces giant SO splitting on semiconductor surfaces.^{25,26} A single Bi bilayer has been studied extensively as it exhibits various topological phases upon structural and chemical modification.^{27–41} Furthermore, Bi-NTs as well as Bi-NT arrays have been experimentally synthesized.^{42–45} Remarkably, we discover that Bi-NT arrays represent a new family of 2D TIs (QSH insulators), as confirmed from first-principles calculations of band topology and 1D helical edge states. The topological order is shown to have originated from the inversion of bonding–antibonding levels of Bi-NT band-edge molecular orbitals, different from atomic-orbital band inversion in conventional TIs⁵ and nanopatterned semiconductors.¹¹ Furthermore, the topological properties of Bi-NT arrays can be systematically tuned by tube size and inter-tube binding, a unique and interesting property absent for conventional TIs. An energy gap of ~ 70 meV is achieved, facilitating possible room-temperature measurement. Practically, the fact that topological edge states are localized on individual nanotubes may pave the way for edge only transport measurement without bulk interference.

The first-principles calculations are performed in the framework of generalized gradient approximations with the Perdew–Burke–Ernzerhof functional using the plane wave basis Vienna ab initio simulation package (VASP) code.^{46,47} All the calculations are carried out with the kinetic energy cutoff of 400 eV on the $3 \times 15 \times 1$ Monkhorst–Pack k -point mesh. A vacuum layer 20 Å thick is used to ensure decoupling between neighboring arrays. All structures are fully optimized until the residual forces are less than 0.01 eV \AA^{-1} . The SOC is included in the self-consistent electronic structure calculation.⁴⁸ The phonon calculations are carried out by using the density functional perturbation theory as implemented in the PHONOPY code.⁴⁹ The topological character is determined by calculating the Z_2 invariant following the approach introduced by Soluyanov and Vanderbilt.⁵⁰

The structure of Bi-NT is formed by a bilayer of Bi atoms that is bonded like a trigonal pyramid in a hexagonal mesh. Fig. 1(a) shows the schematic atomic structure of (7,0) type (zigzag) Bi-NT (see Fig. S1† for the notation of Bi-NTs). A 2D Bi-NT array consists of parallel Bi-NTs lying side by side along the axial direction, as observed experimentally.^{43,44} Fig. 1(b)–(d) show the optimized structural configuration of a Bi-NT array made of (7,0) Bi-NTs, where the tubes are laid in the xz plane with their axes along the z -direction. The (7,0) Bi-NT array has mirror symmetry (M_{010}) and glide plane symmetry ($\{M_{100}|0,0,1/2\}$ and $\{M_{110}|0,0,1/2\}$). The adjacent tubes are weakly bonded *via* van der Waals (vdW) interaction with an interatomic distance of $d_{\text{Bi-Bi}} = 3.10 \text{ \AA}$ (Fig. S2†). The center-to-center intertube separation, *i.e.*, the super periodicity along the x -direction is $a_0 = 13.82 \text{ \AA}$, while the periodicity along the z -direction defined by tube chirality is $z_0 = 7.70 \text{ \AA}$. The intertube binding energy depends on the tube orientation angle (φ) in a periodic fashion due to the D_{14h} symmetry of the tube. With the equilibrium tube orientation set at $\varphi_0 = 0^\circ$, the binding energy oscillates with φ in a period of $\Delta\varphi = 25.71^\circ$ and a rotational activation barrier of ~ 68 meV per atom. Thus, the Bi-NT array is thermally quite stable due to this high rotational energy barrier. We also studied other possible intertube bonding geometries and the topological robustness of the Bi-NT array against structural disorder, and evaluated the stability of Bi-NTs from the calculated phonon spectra (Fig. S3–S5†). Certain Bi-NT arrays with larger superperiodicity, *i.e.*, multiple tubes in one unit cell, have been found slightly more stable than the single-tube lattice but they may not have a global gap (Fig. S3†).

Next, we examine band structure and topological properties of the Bi-NT array. The calculated band structures from the optimized zigzag (7,0) Bi-NT array are shown in Fig. 2(a) without SOC (setting the SOC parameter $\lambda_{\text{SO}} = 0$) and Fig. 2(b) with SOC ($\lambda_{\text{SO}} = 1$), respectively. Without SOC, there is an indirect band gap of ~ 223 meV in between the CBM at Γ and

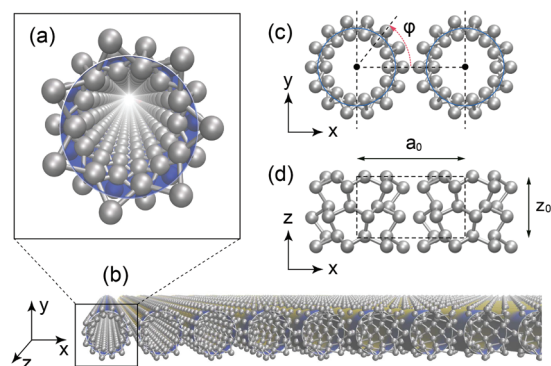


Fig. 1 (a), (b) The schematic atomic structure of a zigzag (7,0) Bi-NT, and a 2D array made of (7,0) Bi-NTs, respectively. Gray balls denote Bi atoms. A circle is depicted in the middle of the bilayer for guidance. There are two different terminations: the side- and end-termination. (c), (d) Side and top views of the Bi-NT array, with dashed lines marking the unit cell. The tube orientation angle φ is shown in (c).

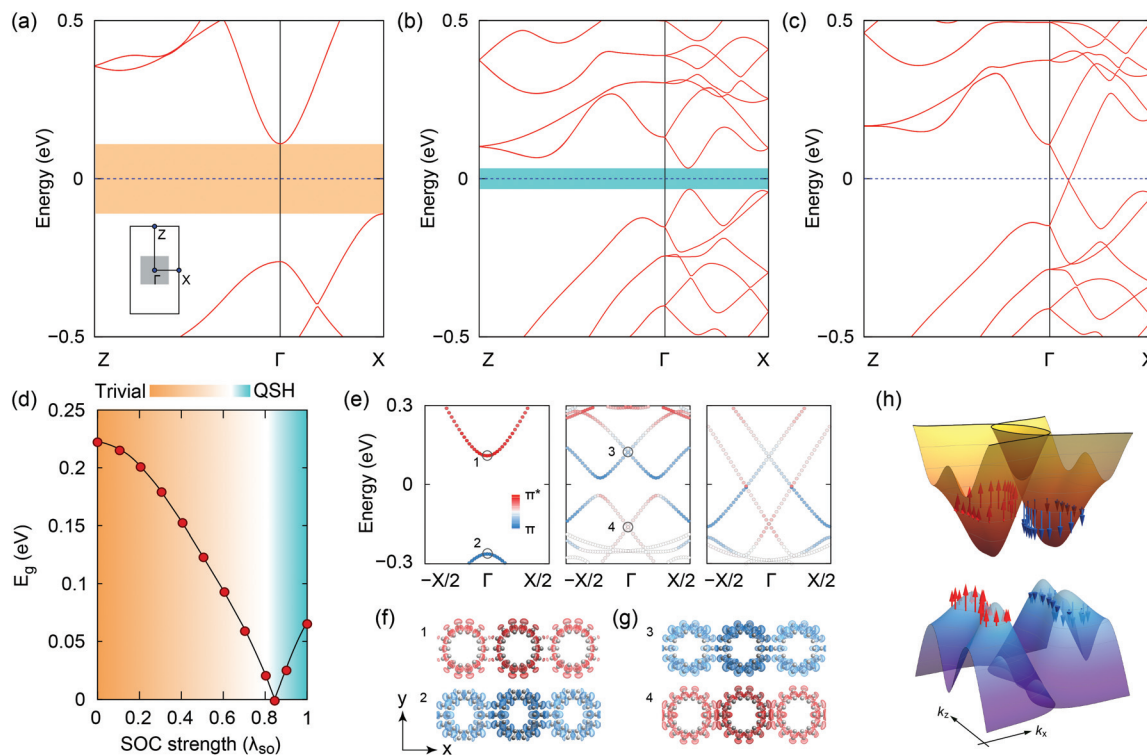


Fig. 2 (a)–(c) Calculated band structure of a (7,0) Bi-NT array with the SOC strength (λ_{SO}) set at $\lambda_{\text{SO}} = 0$, 1 (true value) and 0.84, respectively. The inset in (a) shows the first Brillouin zone (BZ) of the Bi-NT array. (d) The energy gaps as a function of varying SOC strength from 0 to 1. (e) Enlarged band edge structures with the SOC strength set at 0, 1 and 0.84, showing the bonding (π) and anti-bonding (π^*) molecular orbital contribution. The color gradient from blue to red represents varying contributions from bonding to anti-bonding molecular orbitals. (f), (g) The partial charge density plot of the valence and conduction state used in (e) at the Γ point indicated by number. (h) The three-dimensional band plot near the Γ point in (b) as shaded BZ in (a) with the spin texture.

VBM at X; while with SOC, there is a direct band gap of ~ 70 meV located between Γ and X. For band topology, our calculations show that $Z_2 = 1$ (Fig. S6[†]), which surprisingly indicates that the Bi-NT array has a QSH phase. The nontrivial topological order remains but with an increased gap using a hybrid functional calculation (Fig. S7[†]).

To better understand the topological behavior, we have artificially increased the strength of SOC from $\lambda_{\text{SO}} = 0$ to its true value $\lambda_{\text{SO}} = 1$ and monitored the evolution of band structure. Fig. 2(d) shows that the (indirect) gap first decreases continuously with increasing SOC strength and closes at $\lambda_{\text{SO}} = 0.84$; then a (direct) gap reopens with the further increase of SOC. Such a gap closing–reopening process is a typical manifestation of band inversion; the system reaches its quantum critical point at $\lambda_{\text{SO}} = 0.84$, represented by a fully closed gap along the Γ –X direction as shown in Fig. 2(c). This behavior can be understood by an effective model (Fig. S8[†]).

Topological band inversion must be associated with an orbital character exchange between the edge states across the band gap. In a conventional TI of crystalline solids, this is achieved between the CBM and VBM edge states composed of, e.g. s–p, p–p*, or d–p atomic or molecular orbitals of opposite parities. On the other hand, in a crystal, it could be confusing to call the band edge state a molecular orbital. However, in a

nanostructured topological material, as we discover here in the Bi-NT arrays, the concept of a molecular orbital is well defined, and the crystal is formed by bonding between these molecular motifs so that the band edge states are characterized with molecular orbitals acting like a single super atomic orbital. For the Bi-NT arrays, the band edge states are no longer composed of atomic orbitals of known parities. Instead, they are composed of molecular orbitals from a linear combination of many atomic orbitals, whose parity symmetry is not apparent. Furthermore, the zigzag Bi-NT array has no inversion symmetry; hence the parity eigenvalues are not good quantum numbers to define the topological phase. Alternatively, we use band inversion with different orbital characters which is one of the signatures of topological phase transition. Therefore, it is very interesting to examine the molecular orbital character associated with the edge states in the Bi-NT array and how the bonding–antibonding molecular orbitals exchange happens through the band inversion process.

To reveal the underpinning mechanism of band inversion, we show in Fig. 2(e)–(g) the respective bonding characteristics of CBM and VBM edge states along the Γ –X direction for different SOC strengths. A thorough analysis of these band edge states reveals a clear trend of changing molecular orbital characteristics as a function of SOC strength. Without SOC ($\lambda_{\text{SO}} = 0$), the

VBM states are dominated by the bonding molecular orbital of even wavefunction character while the CBM states are dominated by the anti-bonding orbital of odd wavefunction character [see top left panel of Fig. 2(e)]. The molecular bonding and antibonding orbitals are well defined in pristine Bi-NT (Fig. S9†). With SOC ($\lambda_{\text{SO}} = 1$), by contrast, the bonding characteristics are switched, with the anti-bonding orbital now contributing most significantly to the VBM and the bonding orbital to the CBM. At the quantum critical point ($\lambda_{\text{SO}} = 0.84$), both the CBM and VBM edge states share mixed bonding/anti-bonding characteristics. The above analysis clearly indicates that a band inversion has happened with an exchange of opposite molecular orbital character between the CBM and VBM edge states, leading to a QSH phase transition.

We note also a couple of subtle points. For the Bi-NT array, the nontrivial gap is opened at two low-symmetry k -points along Γ - X directions, rather than the usual high-symmetry k -points for conventional TIs. There is a giant Rashba spin splitting (RSS) of bands around the non-trivial gap, as the SOC lifts the degeneracy of energy bands along the Γ - X direction. The giant RSS in the Bi-NT array originates from the strong SOC of Bi atoms and the charge redistribution at the junction point between the neighboring tubes (Fig. S10†), which gives rise to an effective electrical field similar to a field normal to the plane of the Bi bilayer.^{51,52} The RSS induces a peculiar spin texture in the band structure. As shown in Fig. 2(h), near the Γ point, there are two valleys having opposite spins.

After identifying the 2D Bi-NT array as a QSH insulator, we further investigate the features of its non-trivial edge states. As the Bi-NT has a uniaxial symmetry, the structure of a 2D Bi-NT array is highly anisotropic, which has two distinctively different types of edges: one terminated by the sides of the tube and the other by the ends of the tube. A 2D TI will exhibit helical edge states independent of edge orientation and type. Thus, we have calculated edge states of “nanoribbons” made of either a finite number of 16 Bi-NTs, with a ribbon width of 21.9 nm and an infinite length, for the side-termination [Fig. 3(a)] or a finite length of infinite number of tubes, with a ribbon width of 12.1 nm for the end-termination [Fig. 3(b)], respectively. For both cases, the ribbon width is chosen large enough to eliminate coupling between two edges. For the side-terminated edges, one clearly sees the presence of helical edge states centered at the Γ point within the bulk band gap [Fig. 3(c)], where the edge states are completely degenerate due to mirror symmetry. There is an odd number (one) of topologically protected gapless edge states per edge, confirming the existence of the QSH state indicated by the Z_2 calculation above. The real-space charge distribution plotted from the emerged helical edge states shows that they extend four to five tubes into the nanoribbon, as shown in Fig. 3(a). It is related to the localization length (l) of the edge state which is ~ 4.36 nm (~ 3.68 nm) for the side- (end-) termination (Fig. S11†).

Generally, topological edge states are considered robust against edge structural and chemical modifications, because they are protected by bulk band topological order. For the

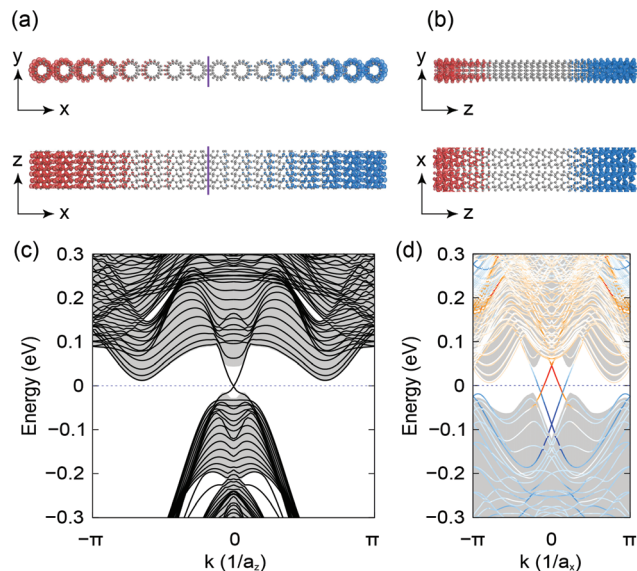


Fig. 3 (a), (b) The structure of “nanoribbons” made of either a finite number of 16 Bi-NTs of infinite length for the side-termination or a finite length of infinite Bi-NTs for the end-termination. The top (lower) panel shows the side (top) view. The purple line indicates the mirror plane (yz plane) for the side termination. The real space charge distribution of topological edge states at the Dirac point are also shown with an isosurface $2 \times 10^{-4} e \text{ \AA}^{-3}$. The red (blue) isosurface indicates the edge states of the left (right) edge. (c), (d) Energy dispersion of edge states for the (7,0) Bi-NT array nanoribbon structure for edge-termination geometry shown in (a) and (b), respectively. Shaded regions denote the energy spectrum of the bulk.

cases of nanostructured materials we study here, one difference is that relatively larger scale structural variations can arise from varying tube diameters and lengths, in addition to local atomic disorder as in conventional atomic crystals. We have found that the topological phase is rather robust against variations in bonding distances and nanotube sizes. Furthermore, we note that the topological edges will remain robust as long as the physical edges are decoupled with negligible inter-edge interactions. For the Bi-NT arrays, this coupling length is ~ 20 nm, which sets a lower limit for tube lengths and diameters.

Also, for the end-terminated edges [Fig. 3(b)], there are two separate sets of edge states [Fig. 3(d)], one from each edge due to broken mirror symmetry. Both sets of helical edge states have their Dirac point located at the Γ point but relatively shifted above and below the Fermi level, indicating a charge transfer between the two edges (*i.e.*, two ends of the tube) due to the inequivalent terminated edges. The fact that the two topological edge states are in different charge states, one of n -type [shown as blue in Fig. 3(d)] and the other of p -type (red), may offer some novel interesting features and new spintronic functionalities, such as the creation of entangled electron–hole pairs *via* inter-edge tunneling, because in principle it enables one to selectively control the conduction of pure spin current from just one edge by doping or gating. For the spin structure of the edge state in both side- and end-termin-

ation setups, we evaluate the expectation values of spin operators $\langle S_\alpha(\mathbf{k}) \rangle = (\hbar/2)\langle \psi(\mathbf{k}) | \sigma_\alpha | \psi(\mathbf{k}) \rangle$ ($\alpha = x, y, z$), where $\psi(\mathbf{k})$ are the wave functions and σ_α the corresponding Pauli matrices. The spin component of the edge state for both side- and end-termination has the out-of-plane (y -direction) component only, showing the helical nature and spin-momentum locking property.

As Fig. 3(a) indicates, in an array of *identical* nanotubes, *topological order makes the bulk tubes in the middle of the array insulating, whereas the boundary tubes outside conducting*. This distinction between the bulk and boundary tubes provides a significant advantage of nanostructured topological materials over the conventional ones in terms of eliminating the bulk contribution to the quantized boundary transport, which has been a long-standing experimental challenge. Specially, it is much easier to address individual tubes than atom rows, and it is possible to place electrodes only on a few conducting boundary tubes at the edge in a two-terminal measurement as illustrated in Fig. 4(a), so that conduction only occurs through these boundary tubes without bulk tube contribution. It also allows for the measurement of pure spin current from just one edge (one side of boundary tubes) with the other edge disconnected.

Another advantage of nanostructured topological materials lies in their high tunability. We found that non-trivial topological order sustains for various Bi-NT arrays, and the properties of the QSH phase in Bi-NT array can be tuned by tube size. Specifically, the band gap varies from 70 meV for the (7,0)

Bi-NT to ~ 20 meV for the (13,0) Bi-NT (Fig. S12[†]). We have confirmed that the QSH phase of the Bi-NT array is preserved on a 2D boron nitride sheet (Fig. S13[†]), which has been used as the substrate to grow graphene or assemble 2D stacked nano-devices. Furthermore, the layout of a nanotube array can be easily controlled by substrate [Fig. 4(b) and (c)]. Curvature or local strains are believed to affect the transport and spin properties. Using curved and patterned substrates, a Bi-NT can be arranged into different curved morphologies, so as to modify its spin properties in the QSH state.^{52–54} The helicity of edge states persists even when the Bi-NT array is bent (Fig. S14[†]). Interestingly, both edges will have the same spin direction in the bent Bi-NT array if the normal directions of the two edges are aligned in parallel. This may provide an efficient way to manipulate the spin-polarized transport using nanostructured topological materials, as shown in Fig. 4(d).

Conclusions

In conclusion, using first-principles calculations we have demonstrated the existence of a nontrivial topological phase in Bi-NT arrays, a nanostructured material with super periodicity. The QSH state emerges from an SOC induced gap opening accompanied by band inversion arising from an exchange of the bonding–antibonding character of nanotube molecular orbitals, instead of the exchange of atomic orbitals in conventional QSH systems. Our findings will foster an exciting highly interdisciplinary new field of “nanostructured topological materials”, by merging together two existing areas of nano-materials and topological physics. It is very much expected that different topological phases can all be extended to a wide range of nanostructured materials, such as 2D TIs in a 2D array of 1D nanotubes and nanowires, 3D TIs in a 3D array of 0D nanodots, as well as their magnetic counterparts. Furthermore, quantized edge conduction can be easily isolated and the properties of this new class of nanostructured topological materials can be highly tuned by size (periodicity of the superlattice), shape and geometry (*e.g.*, chirality of the nanotubes) and inter-nanostructure bonding of the constituent “nanostructural elements”, as well as the way they are assembled together (symmetry of the superlattice).

Conflicts of interest

There are no conflicts to declare.

Acknowledgements

K. H. J. and F. L. acknowledge financial support from DOE-BES (No. DE-FG02-04ER46148). S. H. J. was supported by the National Research Foundation (NRF) through the SRC Center for Topological Matter (Grant No. 2011-0030789). We also acknowledge the Supercomputing Center at USTC, NERSC and

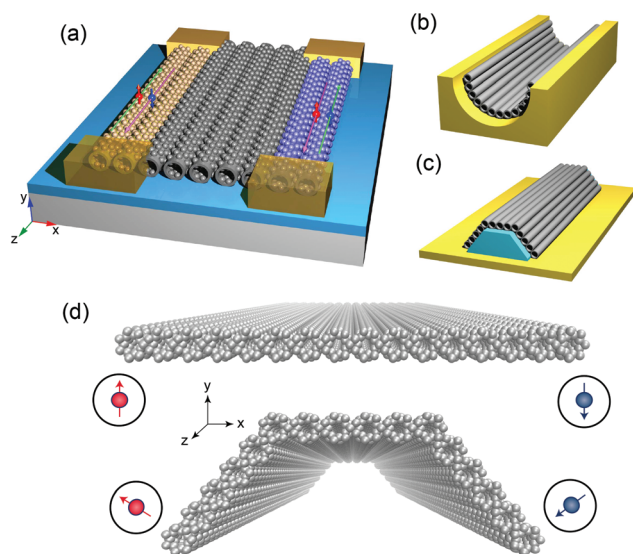


Fig. 4 (a) Schematic setup of transport measurement of the Bi-NT array to isolate quantized edge conductance from bulk contribution. (b), (c) The schematic structures of the Bi-NT array on various patterned substrates. (d) Cross-sectional view of flat and curved (7,0) Bi-NT arrays and corresponding spin orientations of their edge states transporting along $+k_z$. The curved 2D QSH system leads to edge spin rotation. For the flat Bi-NT array, the spin is aligned normal to the ribbon plane (the y -direction); for the curved Bi-NT array, both edges have almost the same spin direction.

CHPC at University of Utah for providing the computing resources.

References

- H. W. Kroto, J. R. Heath, S. C. O'Brien, R. F. Curl and R. E. Smalley, *Nature*, 1985, **318**, 162–163.
- K. S. Novoselov, A. K. Geim, S. V. Morozov, D. Jiang, M. I. Katsnelson, I. V. Grigorieva, S. V. Dubonos and A. A. Firsov, *Nature*, 2005, **438**, 197–200.
- C. L. Kane and E. J. Mele, *Phys. Rev. Lett.*, 2005, **95**, 146802.
- C. L. Kane and E. J. Mele, *Phys. Rev. Lett.*, 2005, **95**, 226801.
- B. A. Bernevig, T. L. Hughes and S. C. Zhang, *Science*, 2006, **314**, 1757–1761.
- M. König, S. Wiedmann, C. Brune, A. Roth, H. Buhmann, L. W. Molenkamp, X. L. Qi and S. C. Zhang, *Science*, 2007, **318**, 766–770.
- H. Zhang, C.-X. Liu, X.-L. Qi, X. Dai, Z. Fang and S.-C. Zhang, *Nat. Phys.*, 2009, **5**, 438–442.
- Y. L. Chen, J. G. Analytis, J.-H. Chu, Z. K. Liu, S.-K. Mo, X. L. Qi, H. J. Zhang, D. H. Lu, X. Dai, Z. Fang, S. C. Zhang, I. R. Fisher, Z. Hussain and Z.-X. Shen, *Science*, 2009, **325**, 178–181.
- P. Gentile, M. Cuoco and C. Ortix, *Phys. Rev. Lett.*, 2015, **115**, 256801.
- S. M. Avdoshenko, P. Koskinen, H. Sevinçli, A. A. Popov and C. G. Rocha, *Sci. Rep.*, 2013, **3**, 1632.
- O. P. Sushkov and A. H. Castro Neto, *Phys. Rev. Lett.*, 2013, **110**, 186601.
- M. Zhou, W. Ming, Z. Liu, Z. Wang, P. Li and F. Liu, *Proc. Natl. Acad. Sci. U. S. A.*, 2014, **111**, 14378–14381.
- Z. F. Wang, K.-H. Jin and F. Liu, *Wiley Interdiscip. Rev.: Comput. Mol. Sci.*, 2017, **7**, e1304.
- Z. F. Wang, Z. Liu and F. Liu, *Phys. Rev. Lett.*, 2013, **110**, 196801.
- Z. F. Wang, K.-H. Jin and F. Liu, *Nat. Commun.*, 2016, **7**, 12746.
- M. S. Bahramy, B. J. Yang, R. Arita and N. Nagaosa, *Nat. Commun.*, 2012, **3**, 679.
- W. Kratschmer, L. D. Lamb, K. Fostiropoulos and D. R. Huffman, *Nature*, 1990, **347**, 354–358.
- C. Ashman, S. N. Khanna, F. Liu, P. Jena, T. Kaplan and M. Mostoller, *Phys. Rev. B: Condens. Matter*, 1997, **55**, 15868–15873.
- X. Roy, C.-H. Lee, A. C. Crowther, C. L. Schenck, T. Besara, R. A. Lalancette, T. Siegrist, P. W. Stephens, L. E. Brus, P. Kim, M. L. Steigerwald and C. Nuckolls, *Science*, 2013, **341**, 157–160.
- W.-L. Ong, E. S. O'Brien, P. S. M. Dougherty, D. W. Paley, C. Fred Higgs Iii, A. J. H. McGaughey, J. A. Malen and X. Roy, *Nat. Mater.*, 2017, **16**, 83–88.
- A. Thess, R. Lee, P. Nikolaev, H. Dai, P. Petit, J. Robert, C. Xu, Y. H. Lee, S. G. Kim, A. G. Rinzler, D. T. Colbert, G. E. Scuseria, D. Tománek, J. E. Fischer and R. E. Smalley, *Science*, 1996, **273**, 483–487.
- P. Delaney, H. J. Choi, J. Ihm, S. G. Louie and M. L. Cohen, *Nature*, 1998, **391**, 466–468.
- S. Kaur, N. Raravikar, B. A. Helms, R. Prasher and D. F. Ogletree, *Nat. Commun.*, 2014, **5**, 3082.
- J. H. Holtz and S. A. Asher, *Nature*, 1997, **389**, 829–832.
- E. Frantzeskakis, S. Pons and M. Gioni, *Phys. Rev. B: Condens. Matter*, 2010, **82**, 085440.
- D. V. Khomitsky and A. A. Chubunov, *J. Exp. Theor. Phys.*, 2014, **118**, 457–466.
- S. Murakami, *Phys. Rev. Lett.*, 2006, **97**, 236805.
- M. Wada, S. Murakami, F. Freimuth and G. Bihlmayer, *Phys. Rev. B: Condens. Matter*, 2011, **83**, 121310.
- T. Hirahara, G. Bihlmayer, Y. Sakamoto, M. Yamada, H. Miyazaki, S.-I. Kimura, S. Blügel and S. Hasegawa, *Phys. Rev. Lett.*, 2011, **107**, 166801.
- F. Yang, L. Miao, Z. F. Wang, M.-Y. Yao, F. Zhu, Y. R. Song, M.-X. Wang, J.-P. Xu, A. V. Fedorov, Z. Sun, G. B. Zhang, C. Liu, F. Liu, D. Qian, C. L. Gao and J.-F. Jia, *Phys. Rev. Lett.*, 2012, **109**, 016801.
- Z. F. Wang, M.-Y. Yao, W. Ming, L. Miao, F. Zhu, C. Liu, C. L. Gao, D. Qian, J.-F. Jia and F. Liu, *Nat. Commun.*, 2013, **4**, 1384.
- S. H. Kim, K.-H. Jin, J. Park, J. S. Kim, S.-H. Jhi, T.-H. Kim and H. W. Yeom, *Phys. Rev. B: Condens. Matter*, 2014, **89**, 155436.
- Z. F. Wang, L. Chen and F. Liu, *Nano Lett.*, 2014, **14**, 2879–2883.
- Z. Song, C.-C. Liu, J. Yang, J. Han, M. Ye, B. Fu, Y. Yang, Q. Niu, J. Lu and Y. Yao, *NPG Asia Mater.*, 2014, **6**, e147.
- J.-J. Zhou, W. Feng, C.-C. Liu, S. Guan and Y. Yao, *Nano Lett.*, 2014, **14**, 4767–4771.
- C.-C. Liu, S. Guan, Z. Song, S. A. Yang, J. Yang and Y. Yao, *Phys. Rev. B: Condens. Matter*, 2014, **90**, 085431.
- H. W. Yeom, S. H. Kim, W. J. Shin, K.-H. Jin, J. Park, T.-H. Kim, J. S. Kim, H. Ishikawa, K. Sakamoto and S.-H. Jhi, *Phys. Rev. B: Condens. Matter*, 2014, **90**, 235401.
- K.-H. Jin and S.-H. Jhi, *Sci. Rep.*, 2015, **5**, 8426.
- T. Lei, K.-H. Jin, N. Zhang, J.-L. Zhao, C. Liu, W.-J. Li, J.-O. Wang, R. Wu, H.-J. Qian, F. Liu and K. Ibrahim, *J. Phys.: Condens. Matter*, 2016, **28**, 255501.
- K.-H. Jin, H. W. Yeom and S.-H. Jhi, *Phys. Rev. B: Condens. Matter*, 2016, **93**, 075308.
- R.-W. Zhang, C.-W. Zhang, W.-X. Ji, S.-S. Yan and Y.-G. Yao, *Nanoscale*, 2017, **9**, 8207–8212.
- Y. Li, J. Wang, Z. Deng, Y. Wu, X. Sun, D. Yu and P. Yang, *J. Am. Chem. Soc.*, 2001, **123**, 9904–9905.
- B. Yang, C. Li, H. Hu, X. Yang, Q. Li and Y. Qian, *Eur. J. Inorg. Chem.*, 2003, **2003**, 3699–3702.
- L. Li, Y. W. Yang, X. H. Huang, G. H. Li, R. Ang and L. D. Zhang, *Appl. Phys. Lett.*, 2006, **88**, 103119.
- R. Boldt, M. Kaiser, D. Köhler, F. Krumeich and M. Ruck, *Nano Lett.*, 2010, **10**, 208–210.
- G. Kresse and J. Furthmüller, *Phys. Rev. B: Condens. Matter*, 1996, **54**, 11169–11186.
- J. P. Perdew, K. Burke and M. Ernzerhof, *Phys. Rev. Lett.*, 1996, **77**, 3865–3868.

- 48 D. Hobbs, G. Kresse and J. Hafner, *Phys. Rev. B: Condens. Matter*, 2000, **62**, 11556–11570.
- 49 A. Togo and I. Tanaka, *Scr. Mater.*, 2015, **108**, 1–5.
- 50 A. A. Soluyanov and D. Vanderbilt, *Phys. Rev. B: Condens. Matter*, 2011, **83**, 235401.
- 51 L. Chen, Z. F. Wang and F. Liu, *Phys. Rev. B: Condens. Matter*, 2013, **87**, 235420.
- 52 K.-H. Jin and S.-H. Jhi, *Phys. Chem. Chem. Phys.*, 2016, **18**, 8637–8642.
- 53 B. Huang, K.-H. Jin, B. Cui, F. Zhai, J. Mei and F. Liu, *Nat. Commun.*, 2017, **8**, 15850.
- 54 L. Z. Zhang, F. Zhai, K.-H. Jin, B. Cui, B. Huang, Z. Wang, J. Q. Lu and F. Liu, *Nano Lett.*, 2017, **17**, 4359–4364.